ELSEVIER

Materials Science and Engineering A242 (1998) 70–76

MATERIALS SCIENCE & ENGINEERING A

R-curve and strength behavior of a functionally graded material

Z.-H. Jin, R.C. Batra *

Department of Engineering Science and Mechanics, Virginia Polytechnic Institute and State University, Blacksburg, VA 24061-0219, USA

Received 24 April 1997; received in revised form 19 June 1997

Abstract

The effects of loading conditions, specimen size and metal particle size on the crack growth resistance curve (R-curve) and residual strength of a ceramic-metal functionally graded material (FGM) are studied based on the crack-bridging concept. It is found that the FGM exhibits strong R-curve behavior when a crack grows from the ceramic-rich region toward the metal-rich region and the residual strength of the FGM with an edge crack at the ceramic side is notch-insensitive. The R-curve is more significant under central tension loading than under pure bending after the crack has grown for a certain amount. However, the residual strength of the FGM decreases with increasing initial crack length more slowly under pure bending than under tension. A larger metal particle usually results in more toughness increase and higher residual strength. Regarding the effect of the specimen size, in terms of the relative crack length a/b, the R-curve is weaker for a smaller specimen when the crack has not grown very deep, and the opposite occurs for deep grown cracks. Based on the real crack growth length, however, the smaller specimen exhibits stronger R-curve behavior. The R-curve also significantly depends on the initial crack size. © 1998 Elsevier Science S.A.

Keywords: Crack growth; Resistance curve; Strength behavior

1. Introduction

Functionally graded materials (FGMs), usually made from ceramics and metals, are promising candidates for future high temperature applications. The ceramic in an FGM offers thermal barrier effects and protects the metal from corrosion and oxidation, and the metallic particles toughen and strengthen it. The compositions and the volume fractions of the constituents in an FGM are varied gradually, thus giving a nonuniform microstructure in the material with continuously graded macro-properties. The macro-nonhomogeneous properties of an FGM reduce stresses when it is subjected to thermal loads [1,2]. Thermal residual stresses can be relaxed in a metal-ceramic layered material by inserting a functionally graded interface layer between the metal and the ceramic [3–6]. When subjected to thermal shocks, FGM coatings suffer significantly less damage than conventional ceramic coatings [7,8]. For exponential variations of material properties, some crack problems for nonhomogeneous solids have been solved under both mechanical [9–11] and thermal loads [12,13]. Interfacial cracking in FGM coatings has been studied in Refs. [14–17]. For general nonhomogeneous materials, Jin and Noda [18] showed that the crack tip fields are identical to those in a homogeneous material if the material properties are continuous and piece-wise continuously differentiable. Hence, the stress intensity factor concept can still be used to study the fracture behavior of FGMs. Based on both the crack-bridging concept and a rule of mixtures, Jin and Batra [19] have shown that an FGM exhibits strong R-curve behavior when a crack grows from the ceramic-rich region toward the metal-rich region and the residual strength of the FGM with an edge crack at the ceramic side is notch-insensitive.

Since crack-bridging may be a major toughening mechanism in some ceramic-metal FGMs and the bridging is expected to be influenced by loading conditions, specimen size and metal particle size, the R-curve and the residual strength of FGMs will also be affected by these factors. We study here the effects of loading conditions, specimen size and metal particle size on the R-curve and the residual strength behavior of a ceramic-metal FGM. We first calculate the stress intensity factors for an edge cracked FGM strip under pure bending, central tension and constant strain loading

* Corresponding author. Fax: +1 540 2314574.

PII S0921-5093(97)00513-3

conditions. Then the R-curves of the FGM are predicted for different values of the metal particle diameter and the specimen width under the three loading conditions. Finally, the residual strength of the cracked FGM is evaluated.

2. An edge crack in an FGM strip

We study plane strain deformations of an infinitely long FGM strip of width b containing an edge crack of length a_0 and subjected at infinity to one of the three loading conditions, i.e. bending moment M, central force N and constant strain ε_s, see Fig. 1. We assume that material properties are uniform in the y-direction, and their variation in the x-direction is given by

$$E' = E'_0 e^{-\gamma(x/b)} \tag{1}$$

$$\mu = \mu_0/[1 + \beta(x/b)], \tag{2}$$

where $E' = E/(1-\nu^2)$, $E'_0 = E_0/(1-\nu_0^2)$, E is Young's modulus, μ the shear modulus, ν Poisson's ratio, and

$$\beta = \mu_0/\mu_1 - 1,\ \gamma = \ln[(E_0/E_1)(1-\nu_1^2)/(1-\nu_0^2)] \tag{3}$$

are constants. Here E_0, ν_0 and μ_0 are the Young's modulus, Poisson's ratio and the shear modulus at $x=0$ and E_1, ν_1 and μ_1 at $x=b$. The Poisson's ratio

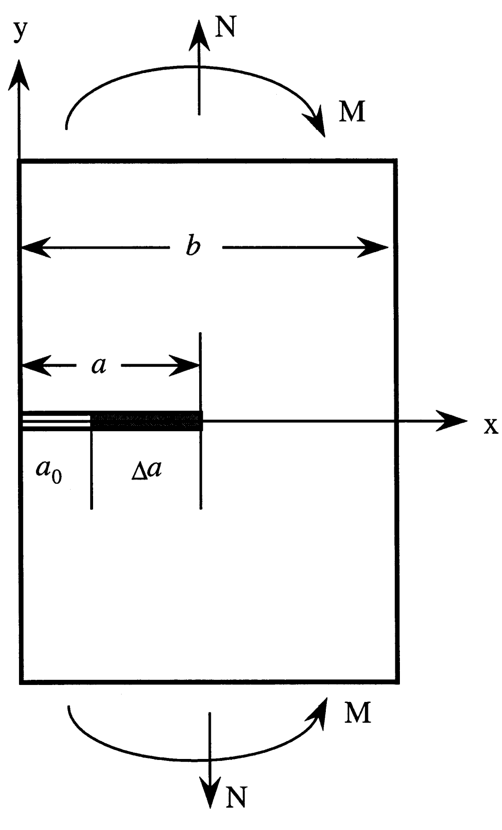

Fig. 1. An edge crack in an FGM strip subjected to loading at infinity.

can be computed from Eq. (1) and Eq. (2) by using $\nu = (E/2\mu - 1)$ and must satisfy the constraint $0 \le \nu \le 0.5$.

The volume fractions of the constituents in a ceramic-metal FGM with properties given by Eq. (1) and (2) may be obtained by using an appropriate micro-mechanical model. We note that the micro-mechanical models developed for macro-homogeneous composites are only approximately valid for FGMs.

For plane strain deformations of the FGM, the Airy stress function, F, satisfies

$$\nabla^2(e^{\gamma(x/b)}\nabla^2 F) = 0 \tag{4}$$

The integral equation for the crack problem can be written as [13]

$$\int_{-1}^{1}\left[\frac{1}{s-r} + K(r,s)\right] e^{-(a_0/b)((1+s)/2)\gamma}\,\phi(s)\,ds = -\frac{2\pi(1-\nu_0^2)}{E_0}p(r), \quad |r| \le 1, \tag{5}$$

$$\phi(x) = \partial v(x,0)/\partial x, \tag{6}$$

where $v(x,0)$ is the displacement in the y-direction at the crack surface, $K(r,s)$ given in Ref. [13] is the kernel singular only at $(r,s) = (-1,-1)$, $r = (2x/a_0 - 1)$, and

$$p(r) = \frac{\gamma^2 e^{-\gamma(x/b)}}{6A_0}\left(A_{12} - \gamma A_{11}\frac{x}{b}\right)\sigma_b, \quad \text{for bending},$$

$$p(r) = \frac{\gamma e^{-\gamma(x/b)}}{A_0}\left[\left(\frac{\gamma^2}{2}A_{11} - \gamma A_{12}\right)\frac{x}{b} + \left(A_{22} - \frac{\gamma}{2}A_{12}\right)\right]\sigma_t, \quad \text{for tension},$$

$$p(r) = \sigma_s e^{-\gamma(x/b)}, \quad \text{for constant strain loading.} \tag{7}$$

The constants A_0 and A_{ij} $(i,j = 1,2)$ are given in Ref. [13], and

$$\sigma_b = 6M/b^2, \qquad \sigma_t = N/b, \qquad \sigma_s = E_0\varepsilon_s/(1-\nu_0^2). \tag{8}$$

According to the singular integral equation method [20,21], a solution of Eq. (5) can be written as

$$\sigma(r) = e^{(a_0/b)((1+r)/2)\gamma}\frac{\psi(r)}{\sqrt{1-r}} \tag{9}$$

where $\psi(r)$ is a continuous and bounded function on the interval $[-1, 1]$. If $\psi(r)$ is normalized by $\sigma^*(1-\nu_0^2)/E_0$, where σ^* is σ_b, σ_t and σ_s for the three loading conditions, respectively, then the normalized stress intensity factor, K^*, at the crack tip is obtained as

$$K^* = \frac{K_I}{\sigma^*\sqrt{\pi a_0}} = -\frac{1}{2}\psi(1). \tag{10}$$

Fig. 2 shows the normalized stress intensity factor (SIF), K^*, versus the normalized crack length a_0/b for both a ZrO_2–Ti FGM and a homogeneous material for the three loading conditions; values of material constants for the FGM are listed in Table 1. For a surface crack problem,

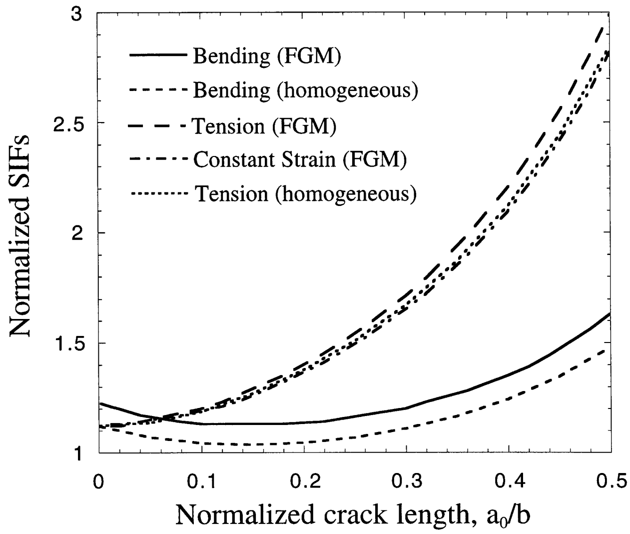

Fig. 2. Normalized stress intensity factors of edge cracked strips of an FGM and homogeneous materials.

$$\lim_{a_0 \to 0} \frac{K_I}{\sigma^* \sqrt{\pi a_0}} = 1.1215 \frac{\sigma_{yy}(0, 0)}{\sigma^*}$$

where σ_{yy} is the stress in the uncracked medium under the given external loads. Using the material data in Table 1, Eqs. (3), (7) and (8), we obtain $\sigma_{yy}(0, 0) = 0.9945\sigma^*$ for the FGM under tension. Therefore,

$$\lim_{a_0 \to 0} \frac{K_I}{\sigma^* \sqrt{\pi a_0}} = 1.1153$$

which agrees well with that obtained from Fig. 2. It is seen from Fig. 2 that the SIF for the FGM varies with a_0/b in the same way as for the homogeneous material. But the SIF of the FGM is higher than that of the homogeneous material under bending and tension loads. This is opposite to the results for thermal loads where the thermal SIF is reduced [13]. However, the reduction in the thermal SIF is mainly due to the thermal conductivity gradient. Though the SIF in the FGM is increased, it will be seen below that this deleterious effect is completely offset by the high fracture toughness of the FGM and as a result, the residual strength of the cracked FGM is much higher than that of the pure ceramic.

This edge crack problem has also been studied in Ref. [10] on the assumption that

$$\mu = \mu_0 e^{\beta x}, \qquad \nu = \nu_0 \tag{11}$$

and their variation of the SIF with a_0/b is similar to that shown in Fig. 2.

3. Crack growth resistance curve (R-curve)

An advantage of FGMs is their high fracture toughness. High crack growth resistance will retard cracking, hence prolong the service life of structural components. Surface cracks at the ceramic side have been observed to propagate in the direction of the variation of material properties when a ceramic-metal FGM is subjected to thermal shocks [8,22,23]. Another major failure mode is cracking perpendicular to the material gradient direction which corresponds to delamination as real FGMs are usually multi-layered materials [22,24,25] and the crack grows along the interface. In our study of R-curve behavior of FGMs, we only consider a Mode-I crack growing in the direction of the material gradation from the ceramic-rich region toward the metal-rich region because cracks are more likely generated first in the ceramic-rich region.

Crack-bridging is believed to be a major toughening mechanism in ductile particulate reinforced brittle matrix composites [26–30]. When a ceramic-metal FGM is fabricated such that the metal inclusions are dispersed in a continuous ceramic phase [24], the crack-bridging concept can be used to study the R-curve of the FGM. However, the crack-bridging concept may not always be appropriate to FGMs as the microstructure in an FGM is generally very different from that in a particulate composite. Jin and Batra [19] studied the R-curve of an Al_2O_3–Ni FGM based on the crack-bridging concept. Since the bridging is expected to be influenced by loading conditions, specimen size and metal particle size, the R-curve and the residual strength of FGMs will also vary with these factors.

After the crack has initiated, it will grow in the ceramic with plastically stretched metal particles behind the crack tip bridging the crack faces. It is assumed that the metal elsewhere is not deformed plastically. A linear softening bridging law

$$\sigma = \sigma_0(1 - \delta/\delta_0) \tag{12}$$

relating the bridging stress σ to the crack opening displacement δ of the bridging zone is used. Here σ_0 is the maximum bridging stress, and δ_0 the maximum crack opening displacement of the bridging zone at which the bridging stress drops to zero. Eq. (12) is appropriate for ductile particle reinforced brittle matrix composites [31].

The integral equation of the crack-bridging problem is [19]

$$L[\phi] = \frac{1 - \nu_0^2}{E_0} [-2\pi p(r) + 2\pi H(r - r_0) V_m(r) \sigma_0], \quad |r| \leq 1 \tag{13}$$

where

$$L[\phi] = \int_{-1}^{1} \left[\frac{1}{s - r} + K(r, s)\right] e^{-(a/b)((1+s)/2)\gamma} \phi(s)\, ds - H(r - r_0) V_m(r) \left(\frac{a}{a_0}\right) a_0^* \int_r^1 \phi(s)\, ds \tag{14}$$

Table 1
Properties of the constituents in a ZrO_2–Ti FGM

	Young's modulus (GPa)	Poisson's ratio	Fracture toughness (MPa $m^{1/2}$)	Tensile strength (MPa)
ZrO_2	150	0.25	2	—
Ti alloy	110	1/3	60	900

is a linear singular integral operator, $H(\ )$ the Heaviside step function, $r_0 = 2a_0/a - 1$, a_0 the initial crack length, Δa the bridging length, and

$$a_0^* = \frac{2\pi a_0(1 - v_0^2)}{E_0\delta_0/\sigma_0} \tag{15}$$

is a nondimensional parameter. $V_m(r)$, determined by Eq. (2) and the three phase model [32], is the metal volume fraction in the FGM, and the loading function $p(r)$ is given by Eq. (7). The crack opening δ is related to ϕ by

$$\delta = -a\int_r^1 \phi(s)\,\mathrm{d}s. \tag{16}$$

The solution of Eq. (13) also has the form of Eq. (9) and can be written as

$$\phi(r) = \mathrm{e}^{(a/b)((1+r)/2)\gamma}\frac{\psi(r)}{\sqrt{1-r}} = \frac{\mathrm{e}^{(a/b)((1+r)/2)\gamma}}{\sqrt{1-r}}\frac{1-v_0^2}{E_0}[\sigma^*\psi_1(1) + \sigma_0\psi_2(1)] \tag{17}$$

where $\psi_1(r)$ and $\psi_2(r)$ are due to σ^* and σ_0, respectively. The stress intensity factor at the crack tip $x = a$, K_{tip}, can be evaluated from

$$K_{\mathrm{tip}} = -\tfrac{1}{2}\sqrt{\pi a}\,[\sigma^*\psi_1(1) + \sigma_0\psi_2(1)]. \tag{18}$$

In Eqs. (17) and (18), σ^* equals, respectively, σ_b, σ_t and σ_s for bending, tensile and uniform strain loading at infinity.

The effective fracture toughness, or R-curve can be evaluated from

$$K_R(a) = \sigma^*\sqrt{\pi a}\,(-\tfrac{1}{2})\psi^0(r)|_{r=1} \tag{19}$$

where the strength σ^* corresponding to

$$K_{\mathrm{tip}} = K_c = \left\{(1 - V_m(a))\frac{1-v_0^2}{1-v^2(a)}\frac{E(a)}{E_0}\right\}^{1/2} K_{\mathrm{IC}}^{\mathrm{ceram}}$$

is

$$\sigma^*(a) = \frac{\sigma_0}{-(1/2)\psi_1(1)}\left\{\frac{K_{\mathrm{IC}}^{\mathrm{ceram}}}{\sigma_0\sqrt{\pi a}}\left[(1 - V_m(a))\frac{1-v_0^2}{1-v^2(a)}\frac{E(a)}{E_0}\right]^{1/2} + \frac{1}{2}\psi_2(1)\right\}, \tag{20}$$

$\psi^0(r) = \mathrm{e}^{-(a/b)((1+r)/2)\gamma}(1-r)^{1/2}\phi^0(r)$ with $\phi^0(r)$ being the solution of Eq. (13) without considering bridging, and $K_{\mathrm{IC}}^{\mathrm{cream}}$ is the fracture toughness of the ceramic in the FGM.

Fig. 3 shows the effective fracture toughness or R-curve for a ZrO_2–Ti FGM. This FGM is particularly attractive [33] because zirconia (ZrO_2) and titanium alloy (Ti) have excellent properties for high temperature applications and they have matched thermal expansions so that the thermal residual stress in the FGM is minimized; the properties of the constituents are summarized in Table 1 and the Ti alloy is assumed to be elastic-perfectly plastic. Following Bao and Zok [31], the maximum bridging stress σ_0 is taken as the maximum value in the model of Mataga [34] and the maximum crack opening δ_0 of the bridging zone is determined by equating the bridging energy of the model of Mataga [34] to $G_b = a_0\delta_0/2$, the bridging energy of the linear softening model (12). σ_0 and δ_0 are thus evaluated as about 900 MPa and 29 μm, respectively, for an average metal particle size, D, of 20 μm. Three initial crack lengths, i.e. $a_0/b = 0.01$, 0.1 and 0.2 with $b = 10$ mm are considered. It is seen from Fig. 3 that the FGM exhibits significant R-curve behavior as the crack grows from the ceramic-rich region toward the metal-rich region. Though the fracture toughness is almost identical when the crack growth initiates under three loading conditions, at a later stage of crack growth the toughness increase is more significant under tension and constant strain loading conditions than that under bending loads. Hence, the R-curve behavior of the FGM is dependent on external loading conditions. We note that the R-curve is due to crack-bridging, and the loading conditions influence the crack opening displacement and thus affect the bridging stress according to Eq. (12). Fig. 4 shows the R-curve versus the crack growth length Δa when a bending moment is applied at far away ends. It is evident that the initial crack size influences the R-curve strongly. This is because a crack with a longer initial length will grow in a region with larger metal volume fraction, resulting in a stronger R-curve. Fig. 5 shows the R-curve for two metal particle sizes under bending. A smaller particle size (average size 10 μm) reduces the increase in toughness. However, the metal particle size can not be too large. In that case, large scale damage in the ceramic may be induced which will degrade the performance of the FGM. Fig. 6 shows the effect of the specimen width on the R-curve under bending. In terms of the relative crack length a/b, the R-curve is weaker for smaller specimens when the crack has not grown very deep. However, the inverse happens for larger crack growths. Based on the real crack growth length Δa, the smaller specimens exhibit stronger R-curve behavior, Fig. 6(b). This is to be expected for FGMs as the metal volume fraction is larger at a fixed crack length a for a smaller specimen resulting in a higher toughness. The R-curve is not a material property as it is affected by loading conditions, specimen size, particle size, and possibly other factors.

When the metal volume fraction becomes large, the crack-bridging may not be the only major mechanism responsible for the change in the toughness and the residual strength discussed below. Extensive plastic deformations of the metal, microcracking, other forms of damage in the ceramic, and the debonding between the ceramic and the metal may occur in a diffusive region around the crack tip. Additional research is needed to understand the constitutive behavior in that region.

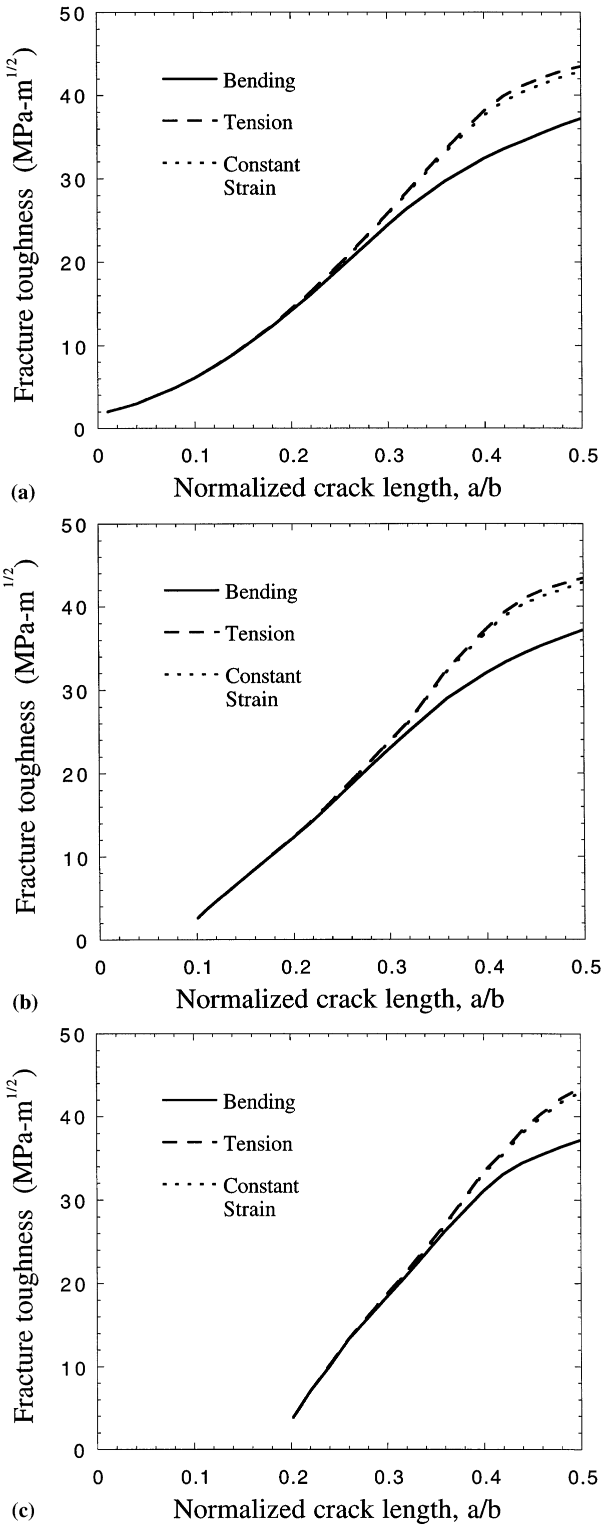

Fig. 3. R-curve of a ZrO_2–Ti FGM: (a) $a_0/b = 0.01$, (b) $a_0/b = 0.1$ and (c) $a_0/b = 0.2$.

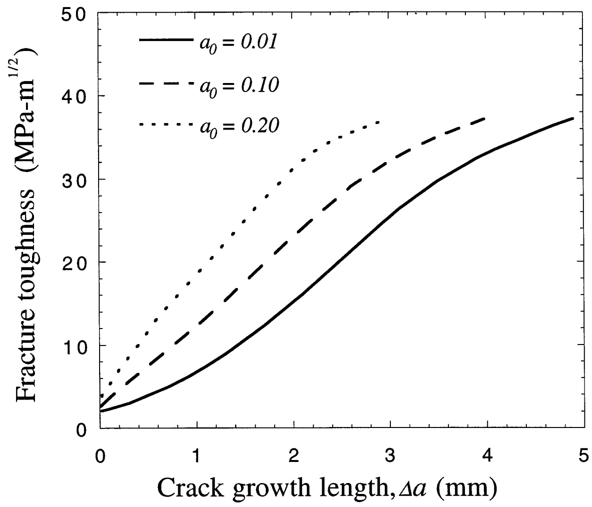

Fig. 4. R-curve of a ZrO_2–Ti FGM: effect of initial crack size (bending loading).

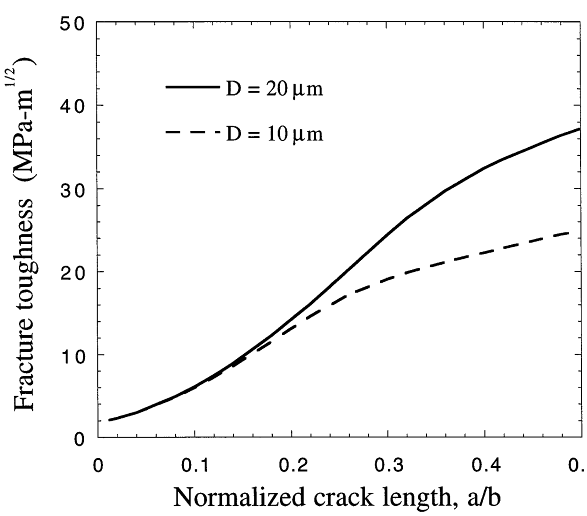

Fig. 5. R-curve of a ZrO_2–Ti FGM: effect of metal particle size (bending loading).

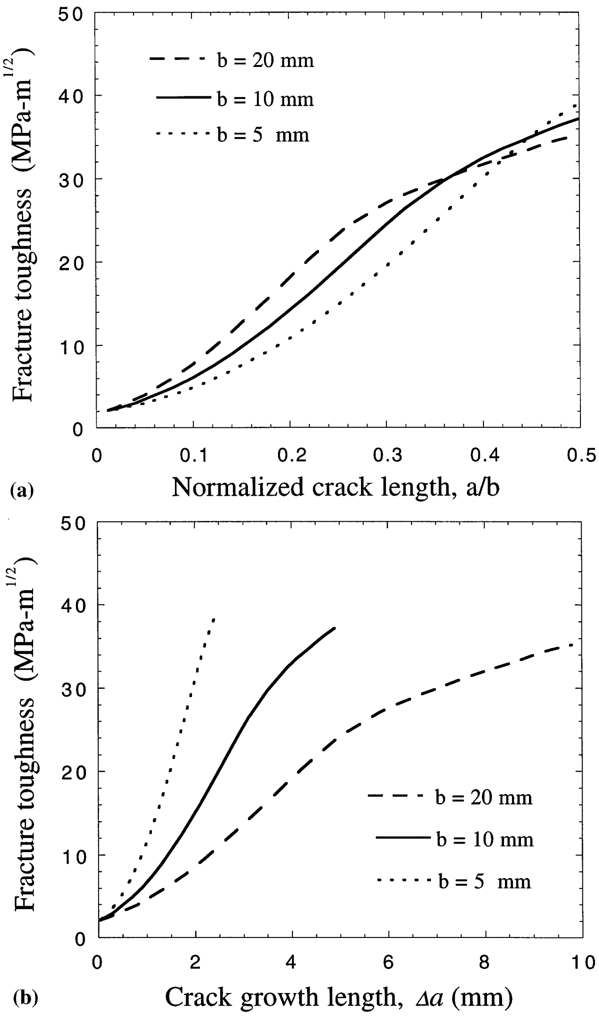

Fig. 6. R-curve of a ZrO_2–Ti FGM: effect of specimen size (bending loading).

4. Residual strength

We do not use the R-curve to calculate the residual strength since it is not a material property. The residual strength corresponding to an initial crack length a_0 is obtained from Eq. (20) as

$$\sigma_R(a_0) = \max_{a \geq a_0} \{\sigma^*(a)\} \tag{21}$$

Figs. 7(a) and (b) show the residual strength of the ZrO_2–Ti FGM as a function of the normalized crack length a_0/b for remote bending and tension loading. It is seen that the residual strength is crack-insensitive for $a_0/b \leq 0.1$ under both loading conditions. The specimen has higher residual strength under bending than that under tension, though the R-curve results are in the opposite order (Fig. 3). The opposite result for the R-curve is possibly due to the larger applied SIF under tension (Fig. 2). The residual strength decreases with a_0/b faster under tension than under bending. A larger particle size gives a higher residual strength. A smaller specimen has higher residual strength than a larger specimen for the same value of the nondimensional crack length a_0/b. It is coincidental that the residual strengths for $b = 10$ mm, $D = 10$ μm and $b = 20$ mm, $D = 20$ μm in Figs. 7(a) and (b) are almost equal.

5. Conclusions

Ceramic-metal FGMs exhibit strong R-curve behavior when a crack grows from the ceramic-rich region toward the metal-rich region. The crack-bridging concept may be applied to study the R-curve of FGMs with a continuous ceramic phase. The R-curve and the residual strength of a ZrO_2–Ti FGM have been calculated and it is found that the R-curve is more significant under central tension loading than under pure bending after the crack has grown by a certain length. The

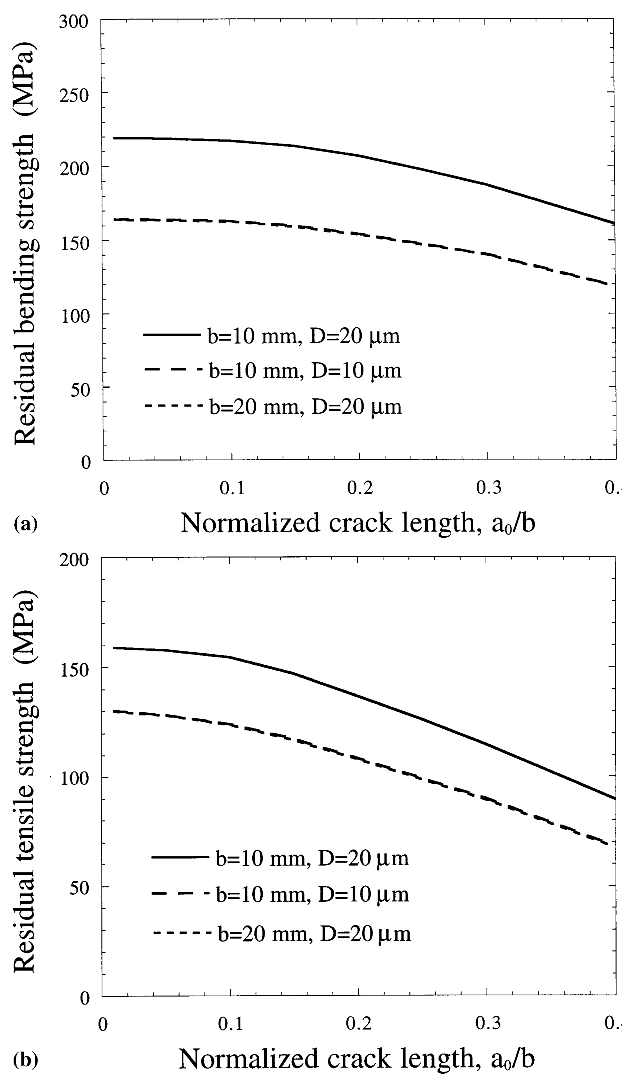

Fig. 7. Residual strength of an edge cracked FGM, (a) bending and (b) tension loading.

residual strength of the FGM decreases with increasing initial crack length more slowly under pure bending than under tension. A larger metal particle size usually results in more toughness increase and higher residual strength. Regarding the effect of the specimen size, in terms of the relative crack length a/b, the R-curve is weaker for a smaller specimen when the crack has not grown very deep; the inverse occurs for deeper grown cracks. Based on the real crack growth length, however, the smaller specimen always exhibits stronger R-curve behavior. The R-curve also strongly depends on the initial crack size.

References

[1] D.P.H. Hasselman, G.E. Youngblood, J. Am. Ceram. Soc. 61 (1978) 49–52.

[2] N. Noda, T. Tsuji, Steady thermal stresses in a plate of a functionally gradient material, in: M. Yamanouchi, M. Koizumi, T. Hirai, I. Shiota (Eds.), Proc. 1st Int. Symp. on Functionally Gradient Materials, Sendai, Japan, 1990, pp. 339–344.

[3] A. Kawasaki, R. Watanabe, J. Jpn. Inst. Met. 51 (1987) 525–529.

[4] J.T. Drake, R.L. Williamson, B.H. Rabin, J. Appl. Phys. 74 (1993) 1321–1326.

[5] A.E. Giannakopoulos, S. Suresh, M. Finot, M. Olsson, Acta Metall. Mater. 43 (1995) 1335–1354.

[6] K.S. Ravichandran, Mater. Sci. Eng. A201 (1995) 269–276.

[7] Y. Kuroda, K. Kusaka, A. Moro, M. Togawa, Evaluation tests of ZrO_2/Ni functionally gradient materials for regeneratively cooled thrust engine applications, in: J.B. Holt, M. Koizumi, T. Hirai, Z.A. Munir (Eds.), Ceramic Transactions, Vol. 34, Functionally Gradient Materials, American Ceramic Society, Westerville, OH, 1993, pp. 289–296.

[8] H. Takahashi, T. Ishikawa, D. Okugawa, T. Hashida, Laser and plasma-ARC thermal shock/fatigue fracture evaluation procedure for functionally gradient materials, in: G.A. Schneider, G. Petzow (Eds.), Thermal Shock and Thermal Fatigue Behavior of Advanced Ceramics, Kluwer Academic, Dordrecht, 1993, pp. 543–554.

[9] F. Delale, F. Erdogan, ASME J. Appl. Mech. 50 (1983) 609–614.

[10] F. Erdogan, B.H. Wu, Analysis of FGM specimens for fracture toughness testing, in: J.B. Holt, M. Koizumi, T. Hirai, Z.A. Munir (Eds.), Ceramic Transactions, Vol. 34, Functionally Gradient Materials, American Ceramic Society, Westerville, OH, 1993, pp. 39–46.

[11] P. Gu, A.J. Asaro, Int. J. Solids Struct. 34 (1997) 1–17.

[12] Z.-H. Jin, N. Noda, Int. J. Solids Struct. 31 (1994) 203–218.

[13] Z.-H. Jin, R.C. Batra, J. Thermal Stresses 19 (1996) 317–339.

[14] K. Kokini, Y.R. Takeuchi, Interface cracks in thermally loaded multilayer ceramic coatings, in: F. Erdogan (Ed.), Fracture Mechanics, Vol. 25, ASTM STP 1220, American Society for Testing and Materials, Philadelphia, 1995, pp. 177–190.

[15] G. Bao, H. Cai, Acta Mater. 45 (1997) 1055–1066.

[16] Y.F. Chen, F. Erdogan, J. Mech. Phys. Solids 44 (1996) 771–787.

[17] Z.-H. Jin, R.C. Batra, Int. J. Eng. Sci. 34 (1996) 1705–1716.

[18] Z.-H. Jin, N. Noda, ASME J. Appl. Mech. 61 (1994) 738–740.

[19] Z.-H. Jin, R.C. Batra, J. Mech. Phys. Solids 44 (1996) 1221–1235.

[20] N.I. Muskhelishvili, Singular Integral Equations, Noordhoff, Groningen, 1953.

[21] G.D. Gupta, F. Erdogan, ASME J. Appl. Mech. 41 (1974) 1001–1006.

[22] A. Kawasaki, R. Watanabe, Fabrication of disk-shaped functionally gradient materials by hot pressing and their thermomechanical performance, in: J.B. Holt, M. Koizumi, T. Hirai, Z.A. Munir (Eds.), Ceramic Transactions, Vol. 34, Functionally Gradient Materials, American Ceramic Society, Westerville, OH, 1993, pp. 157–164.

[23] Y. Shinohara, Y. Imai, S. Ikeno, I. Shiota and T. Fukushima, Thermal stability of plasma sprayed Ni-Cr-Al-Y/PSZ FGM in uniform and gradient temperature fields, in: J.B. Holt, M. Koizumi, T. Hirai, Z.A. Munir (Eds.), Ceramic Transactions, Vol. 34, Functionally Gradient Materials, American Ceramic Society, Westerville, OH, 1993, pp. 255–262.

[24] B.H. Rabin, R.J. Heaps, Powder processing of Ni–Al_2O_3 FGM, in: J.B. Holt, M. Koizumi, T. Hirai, Z.A. Munir (Eds.), Ceramic Transactions, Vol. 34: Functionally Gradient Materials, American Ceramic Society, Westerville, OH, 1993, pp. 173–180.

[25] K. Tanihara, Y. Miyamoto, K. Matsushita, X. Ma, A. Kawasaki, R. Watanabe, K. Hirano, Fabrication of Cr_3C_2/Ni functionally gradient materials by gas-pressure combustion sintering, in: J.B. Holt, M. Koizumi, T. Hirai, Z.A. Munir (Eds.), Ceramic Transactions, Vol. 34, Functionally Gradient Materials, American Ceramic Society, Westerville, OH, 1993, pp. 361–369.

[26] V.D. Krstic, Philos. Mag. A 48 (1983) 695–708.

[27] A.G. Evans, R.M. McMeeking, Acta Metall. 34 (1986) 2435–2441.

[28] L.S. Sigl, P.A. Mataga, B.J. Dalgleish, R.M. McMeeking, A.G. Evans, Acta Metall. 36 (1988) 945–953.

[29] B. Budiansky, J.C. Amazigo, A.G. Evans, J. Mech. Phys. Solids 36 (1988) 167–187.

[30] G. Bao, C.Y. Hui, Int. J. Solids Struct. 26 (1990) 631–642.

[31] G. Bao, F. Zok, Acta Metall. Mater. 41 (1993) 3515–3524.

[32] R.M. Christensen, K.H. Lo, J. Mech. Phys. Solids 27 (1979) 315–330.

[33] Y. Obata, N. Noda, Transient thermal stresses in a plate of functionally gradient material, in: J.B. Holt, M. Koizumi, T. Hirai, Z.A. Munir (Eds.), Ceramic Transactions, Vol. 34, Functionally Gradient Materials, American Ceramic Society, Westerville, OH, 1993, pp. 403–410.

[34] P.A. Mataga, Acta Metall. 37 (1989) 3349–3359.